Spreadsheets in Education (eJSiE)

Volume 7 | Issue 2 Article 4

March 2014

Assessment of the Potential for Earthquake-Induced Liquefaction in Granular Soils

Salah Sadek
American University of Beirut, salah@aub.edu.lb

Shadi Najjar
American University of Beirut, sn06@aub.edu.lb

Yassin Mostapha
American University of Beirut

Mostapha Mostapha
American University of Beirut

Assessment of the Potential for Earthquake-Induced Liquefaction in Granular Soils

Abstract
The assessment of the potential for an earthquake-induced loss of strength (liquefaction) of a granular deposit involves methods which are based on empirical observations, field and lab characterization data and associated analyses. These methods constitute an evolving state of knowledge/practice and involve systematic yet tedious data interpretation, reduction, correction and analysis. For one time/one point calculations these processes can be done by hand, yet they prove to be time consuming with the possibility of introducing unwanted errors at one or more of the many steps involved. The idea of relying on spreadsheets to address these shortcomings is not new. However, past efforts have included one method, with some cases ignoring effects of some important parameters or new methodologies to avoid the added complexity. The approach/tool developed and presented in this paper (*LiqFactory 1.0*) was motivated by, and developed and tested in the context of, a course on geotechnical earthquake engineering with the objective of presenting students with a platform for exploring and understanding the liquefaction phenomenon and the various state-of-the-practice tools available to assess it. The tool relies on standard penetration test (SPT) or cone penetration test (CPT) field test results, soil characteristic properties and earthquake data. Test specific corrections for various field parameters are applied along with other adjustments associated with soil characteristics/composition. In this paper, a concise technical background is presented followed by a thorough discussion of different methods used in programming the spreadsheet and resolving the many problems faced in developing it. In addition, the criteria used in programming the spreadsheets are presented, and finally an illustrative example application is provided to showcase the different features of the tool developed.

Keywords
Earthquakes, Granular Soils, Liquefaction, Settlement, Spreadsheets

Cover Page Footnote
Acknowledgements The authors would like to acknowledge the Lebanese National Council for Scientific Research (LNCSR) and the University Research Board (URB) at the American University of Beirut for funding this work.

Assessment of the Potential for Earthquake-Induced Liquefaction in Granular Soils

Abstract

The assessment of the potential for an earthquake-induced loss of strength (liquefaction) of a granular deposit involves methods which are based on empirical observations, field and lab characterization data and associated analyses. These methods constitute an evolving state of knowledge/practice and involve systematic yet tedious data interpretation, reduction, correction and analysis. For one time/one point calculations these processes can be done by hand, yet they prove to be time consuming with the possibility of introducing unwanted errors at one or more of the many steps involved. The idea of relying on spreadsheets to address these shortcomings is not new. However, past efforts have included one method, with some cases ignoring effects of some important parameters or new methodologies to avoid the added complexity. The approach/tool developed and presented in this paper (*LiqFactory 1.0*) was motivated by, and developed and tested in the context of, a course on geotechnical earthquake engineering with the objective of presenting students with a platform for exploring and understanding the liquefaction phenomenon and the various state-of-the-practice tools available to assess it. The tool relies on standard penetration test (SPT) or cone penetration test (CPT) field test results, soil characteristic properties and earthquake data. Test specific corrections for various field parameters are applied along with other adjustments associated with soil characteristics/composition. In this paper, a concise technical background is presented followed by a thorough discussion of different methods used in programming the spreadsheet and resolving the many problems faced in developing it. In addition, the criteria used in programming the spreadsheets are presented, and finally an illustrative example application is provided to showcase the different features of the tool developed.

Keywords: Earthquakes, Liquefaction, Granular Soils, Spreadsheets.

1. Introduction and Background

Soil liquefaction has been at the center of Geotechnical Earthquake Engineering research, education and practice for the last forty years or so. This phenomenon is associated with the generation of large pore-water pressures in granular soils during seismic shaking, resulting in a reduction of effective particle to particle contact (effective stress) and a consequent loss of strength. The interest in studying the phenomenon of liquefaction was sparked by the devastating effects of the Alaska and Niigata earthquakes (1964) which contributed to widespread "liquefaction-induced" damage (Kramer 1995). One of the first approaches suggested to evaluate liquefaction potential was developed by Seed and Idriss (1971; 1982). Their "simplified procedure" became the standard of practice throughout most of the world.

In 1996 a workshop was convened by Professors Youd and Idriss with 20 experts to review the state of practice of liquefaction assessment and to develop consensus on updates and revisions to the simplified procedure. The recommendations of the workshop were published in Youd et al. (2001).

Liquefaction has been implicated in settlement and structural failure in several recent events. In 1999, two major earthquakes hit the cities of Adapazari and Kocaeli in Turkey causing widespread soil liquefaction. Also in 1999, widespread liquefaction-induced damages occurred in the cities of Wu Feng, Yuan Lin and Nantou during the Chi-Chi (Taiwan) Earthquake. In all four cities, significant liquefaction-induced settlements and bearing capacity failures of shallow-founded structures were documented. These new earthquakes among others provided additional data for testing the effectiveness of the liquefaction assessment procedures and updating them. A major effort in this direction was made by R. Seed et al. (2003) who analyzed results from approximately 450 liquefaction (and "non-liquefaction") field case histories and developed new correlations for the likelihood of initiation (or "triggering") of soil liquefaction. Further work was reported by Idriss and Boulanger (2008) based on a comprehensive database of liquefaction-related cases and presented a modified method for assessing the initiation of liquefaction in granular soils.

The availability of a number of methods for assessing liquefaction potential in granular soils, which in some cases yield contradictory outcomes, has led practicing engineers to raise some questions regarding the reliability of the results and associated design decisions. Since most of the available methods rely on empirical graphs, using them typically favors a manual approach, where parameters are read from the appropriate figures. This is time consuming, especially if a number of parameters need to be varied in the liquefaction assessment.

The various methods and procedures presented in detail in section 2, were programmed into a Microsoft Excel spreadsheet that automates the liquefaction analyses, in an attempt to clarify the relative importance of key elements and simplify their use in engineering education and practice. The user is prompted to enter data related to the soil profile and properties in a user-friendly environment, and the solution of the liquefaction analysis is presented for the different methods programmed. This allows for a quick and visual assessment/comparison of the results of different liquefaction analysis methods for large datasets with minimum effort and potential for error.

2. Methods for the Assessment of Liquefaction Potential

The evaluation of the liquefaction potential of soils necessitates the quantification of the following two "parameters": (1) the seismic "loading" imposed on a soil layer, expressed in terms of the Cyclic Stress Ratio (CSR); and (2) the capacity of the soil to resist liquefaction, expressed in terms of the Cyclic Resistance Ratio (CRR). The factor of safety (FS) against liquefaction could then be defined as the ratio of the CRR to the CSR. The state-of-the-practice methods for the assessment of liquefaction potential relate in situ soil indices, such as the standard penetration test (SPT) or the cone penetration test (CPT) or Shear wave velocity measurements, to observed liquefaction *occurrence* or *non-occurrence* during major earthquakes. The methods presented in the sections below are restricted to SPT and CPT based approaches. The nomenclature and parameter definitions are used are they appear in the original method/reference.

2.1. SPT-Based Liquefaction Approaches

2.1.1. Youd et al. (2001) Method

In the method presented by Youd et al. (2001), the CSR is calculated according to Equation-1 as:

$$CSR = 0.65 \frac{a_{max}}{g} \frac{\sigma_{vo}}{\sigma'_{vo}} r_d \qquad (1)$$

where a_{max} is the peak horizontal acceleration generated by the earthquake at the ground surface; g is the acceleration of gravity; σ_{vo} and σ'_{vo} are the total and effective vertical stresses respectively; and r_d is a stress reduction coefficient function of the depth below the ground surface, z, in meters:

$$r_d = \frac{(1.000 - 0.4113\, z^{0.5} + 0.04052\, z + 0.001753\, z^{1.5})}{(1.000 - 0.4177\, z^{0.5} + 0.05729\, z - 0.006205\, z^{1.5} + 0.001210\, z^{2})} \qquad (2)$$

In the method, the Cyclic Resistance Ratio (CRR) for a reference earthquake of magnitude M_w = 7.5 ($CRR_{7.5}$) is obtained graphically from Figure-1 as a function of the corrected standard penetration number $(N_1)_{60}$, which is a normalized value of penetration resistance to an effective stress of 1 atmosphere and 60% efficiency of the driving hammer. As shown in Figure-1, relationships between the CRR and $(N_1)_{60}$ (solid/dashed lines) are provided for clean sands, sands with 15% fines, and sands with 35% fines. The lines represent the boundaries between liquefaction *occurrence* and *non-occurrence*. Combinations of various applied CSRs and in-situ resistances (SPT-$(N_1)_{60}$, in this case) would plot either on, above or below the respective curve indicating potential behavior. For example, Figure-1 indicates that soils with $(N_1)_{60} \geq 30$ are too dense to liquefy and are as such classified as "non-liquefiable" in the Youd et al. (2001) procedure.

The Factor of Safety against liquefaction is determined from Equation-3 which incorporates a magnitude scaling factor (MSF) that allows the application of the procedure for earthquakes with magnitudes different than 7.5, and an overburden pressure correction factor (K_σ):

$$FS = \frac{CRR_{7.5}}{CSR} MSF\, K_\sigma \qquad (3)$$

Idriss (1995) and Andrus and Stokoe (1997) proposed sets of MSF values as indicated in Table-1. For earthquakes with magnitudes less than 7.5, Youd et al. (2001) recommend that the MSF be taken as the average value from the two references. Otherwise, the MSF is determined in accordance with the Idriss (1995) recommendations.

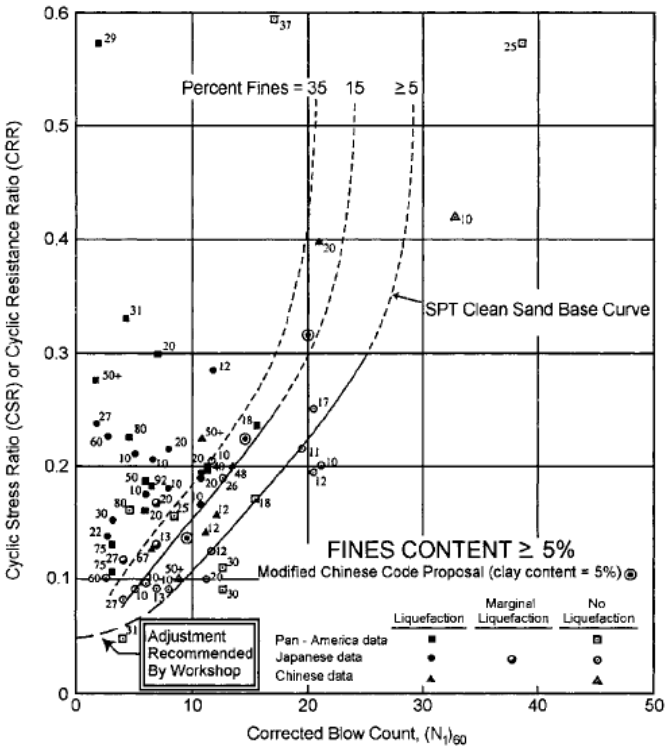

Figure 1: SPT Clean-Sand Base Curve and Curves for Fines Content = 15% and 35% for Magnitude 7.5 Earthquakes with Data from Liquefaction Case Histories (from Youd et al. 2001)

Youd et al. (2001) recommend that the overburden pressure correction factor (K_σ) be evaluated from Equation-4 such that:

$$K_\sigma = (\sigma'_{vo}/P_a)^{(f-1)} \tag{4}$$

where σ'_{vo} is the effective vertical stress; P_a is the atmospheric pressure (same units as σ'_{vo}) and f is an exponent that depends on the site conditions as reflected by the relative density (ref. Table-2). It should be noted that the relative density is generally determined based on correlations with the Standard Penetration N-value $N_{1,60}$ (ref. Table-3).

Table 1: Magnitude scaling factors proposed by Idriss (1995 Seed Memorial Lecture) and Andrus and Stokoe (1997)

Mw	MSF (Idriss)	MSF (Andrus and Stokoe)
5.5	2.2	2.8
6	1.76	2.1
6.5	1.44	1.6
7	1.19	1.25
7.5	1	1
8	0.84	0.8
8.5	0.72	0.65

Table 2: *f* values as a function of the relative density

Dr (%)	f
40	0.8
60	0.7
80	0.6

Table 3: Relationship between $N_{1,60}$ and relative density D_r

$(N_1)_{60}$	D_r (%)	$(N_1)_{60}$	D_r (%)
3	30	20	70
6	40	25	80
10	50	30	90
14	60		

2.1.2. Seed et al. (2003) Method

In the Seed et al. (2003) method, the Cyclic Stress Ratio (CSR*) is given by Equation-5:

$$CSR^* = 0.65 \frac{a_{max}}{g} \frac{\sigma_v}{\sigma'_v} r_d \frac{1}{DWF_M} \frac{1}{K_\sigma} \quad (5)$$

where r_d is defined as the nonlinear stress reduction coefficient and determined from Figure-2, DWF_M is the magnitude-correlated duration weighting factor given by Figure-3a, and M_w is the earthquake magnitude. The factor K_σ is referred to as the overburden correction factor which could be evaluated from Figure-3b as a function of the vertical effective stress σ'_v.

The Cyclic Resistance Ratio (CRR) for the Seed et al. (2003) method is determined based on a probabilistic approach, where the relationships between CRR and $N_{1,60,cs}$ for different probabilities of liquefaction are presented in Equation-6. The parameter $N_{1,60,cs}$ is calculated according to Equations 7 to 10 as a function of the fines content (FC) and $N_{1,60}$ such that:

$$CRR = exp\left[\frac{(N_{1,60} * (1 + 0.004 * FC) - 29.53 * \ln(M_w) - 3.7 \ln\left(\frac{\sigma_v'}{P_a}\right) + 0.05 * FC + 16.85 + 2.7\emptyset^{-1}(P_l)}{13.32}\right] \quad (6)$$

$$N_{1.60,cs} = N_{1,60}\, C_{Fines} \quad (7)$$

Where $C_{\text{Fines}} = 1$ for FC ≤ 5% (8)

$C_{\text{Fines}} = (1 + 0.004\ \text{FC}) + 0.05\left(\frac{\text{FC}}{\text{N}_{1,60}}\right)$ for FC ≥ 5% and FC ≤ 35% (9)

$\text{N}_{1.60,\text{cs}} = \text{N}_{1,60} + 6$ for FC ≥ 35% (10)

Seed et al. (2003) recommend the use of a probability of liquefaction of 15% in the determination of the CRR to evaluate a factor of safety against liquefaction $FS_{liq}=CRR/CSR^*$ that is considered equivalent to conventional deterministic approaches for liquefaction assessment.

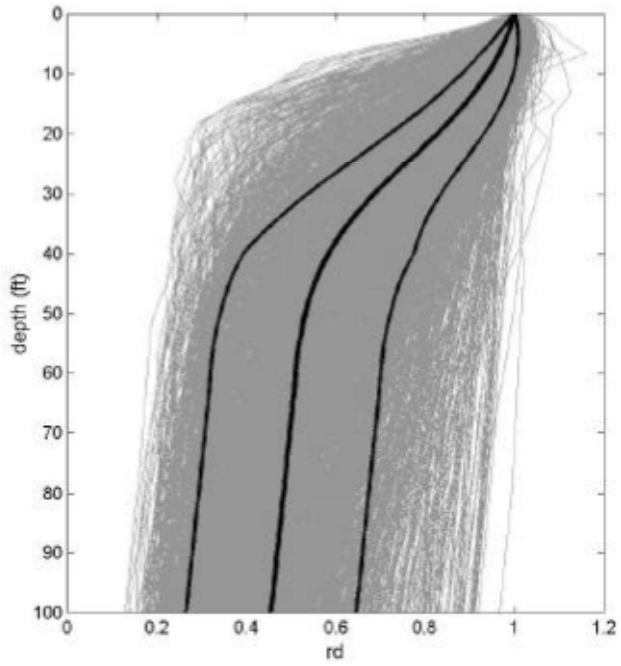

Figure 2: Mean and ± 1 Standard Deviation r_d Values for Response Analyses for 2,153 Combinations of Site Conditions and Ground Motions (Seed et al. 2003).

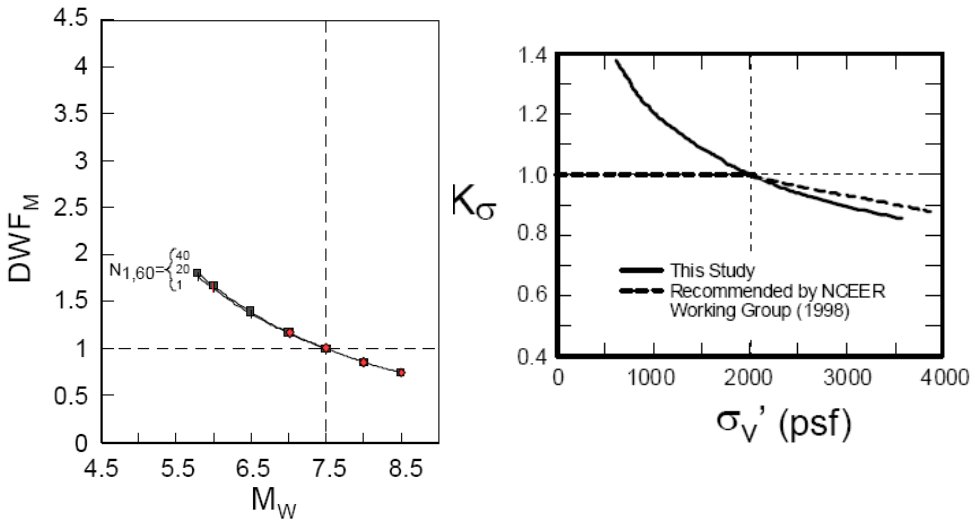

(a) (b)

Figure 3: (a) Recommended magnitude-correlated duration weighting factor as a function of $N_{1,60}$ and (b)Values of K_σ as a function of σ'_v (Seed et al. 2003)

2.1.3. Idriss and Boulanger (2008) Method

In the Idriss and Boulanger (2008) liquefaction approach, the cyclic stress ratio (CSR*) that is corrected for $M_w = 7.5$ and $\sigma'_v = 1$ atm is given by Equation-11 as:

$$CSR_{M=7.5,\sigma'_{vc}=1} = 0.65 \frac{a_{max}}{g} \frac{\sigma_{vc}}{\sigma'_{vc}} r_d \frac{1}{MSF} \frac{1}{K_\sigma} \tag{11}$$

where r_d is calculated using equations 12 to 14 as a function of z and the earthquake magnitude as:

$$r_d = exp[\alpha(z) + \beta(z)M] \tag{12}$$

$$\alpha(z) = -1.012 - 1.126\, sin\left(\frac{z}{11.73} + 5.133\right) \tag{13}$$

$$\beta(z) = 0.106 + 0.118\, sin\left(\frac{z}{11.28} + 5.142\right) \tag{14}$$

MSF is the magnitude scaling factor given by Equation 15 as:

$$MSF = 6.9 \exp\left(\frac{-M}{4}\right) - 0.058 \leq 1.8 \tag{15}$$

K_σ is the overburden correction factor given by Equations 16 and 17:

$$K_\sigma = 1 - C_\sigma \ln\left(\frac{\sigma'_{vc}}{P_a}\right) \leq 1.1 \tag{16}$$

$$C_\sigma = \frac{1}{18.9 - 2.55\sqrt{(N_1)_{60}}} \leq 0.3 \tag{17}$$

The Cyclic Resistance Ratio (CRR) in the Idriss and Boulanger (2008) approach is calculated according to Equation-18 as a function of $(N_1)_{60cs}$ which includes a correction for fines content FC as indicated in Equation-19.

$$CRR_{M=7.5,\sigma'_{vc}=1} = \exp\left(\frac{(N_1)_{60cs}}{14.1} + \left(\frac{(N_1)_{60cs}}{126}\right)^2 - \left(\frac{(N_1)_{60cs}}{23.6}\right)^3 + \left(\frac{(N_1)_{60cs}}{25.4}\right)^4 - 2.8\right) \quad (18)$$

$$(N_1)_{60cs} = (N_1)_{60} + \exp\left(1.63 + \frac{9.7}{FC + 0.01} - \left(\frac{15.7}{FC + 0.01}\right)^2\right) \quad (19)$$

The Factor of Safety against liquefaction is then determined as:

$$FS_{liq} = \frac{CRR_{M=7.5,\sigma'_{vc}=1}}{CSR_{M=7.5,\sigma'_{vc}=1}} \quad (20)$$

2.2. Comparison of SPT-blow Corrections between the Three Methods

The correction factors of the field SPT N-value as recommended by each of the three methods are presented in Table 4. C_N is the correction factor for overburden pressure, C_R is the correction factor for rod length, C_S is the correction factor for the sampler, C_E is the correction factor for the hammer efficiency and C_B is the correction factor for the borehole diameter.

2.3. CPT-Based Liquefaction Approaches

2.3.1. Youd et al. (2001) Method

Youd et al. (2001) presented a CPT-based liquefaction procedure that is founded on the Robertson and Wride (1998) method for direct determination of CRR for clean sands (FC< 5%) from CPT data (Figure-5). They also included a correction factor for "grain characteristics" for sands with fines. Adjustments for fines are based on combinations of sleeve friction ratios and tip resistances in such a manner that the "clean sand" boundary curve of Figure-5 is adjusted based on a composite parameter I_C (Youd et al. 2001). The recommended "fines" correction is a nonlinear function of I_C, and ranges from a factor K_C = 1.0 at I_C = 1.64, to a maximum value of K_C = 3.5 at I_C = 2.60.

Table 4: Correction factors of SPT-blow recommended by each of the three methods

	Cetin & Seed (2004)		Idriss & Boulanger (2008)		Youd et al. (2001)	
C_N	$C_N = \left(\frac{P_a}{\sigma'_v}\right)^{0.5}$ $C_N \leq 1.7$		$C_N = \left(\frac{P_a}{\sigma'_v}\right)^{0.784-0.0768\sqrt{N_{1,60}}}$ $C_N = \left(\frac{P_a}{\sigma'_v}\right)^{1.388-0.249(q_{c1N})^{0.264}}$ $C_N \leq 1.7$		$C_N = \frac{2.2}{1.2+\frac{\sigma'_v}{P_a}}$ $C_N \leq 1.7$	
C_R	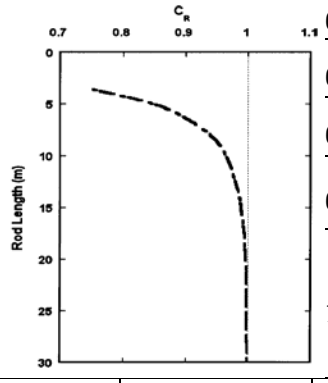		0.75	Rod length < 3 m	0.75	Rod length < 3 m
			0.80	Rod length 3 – 4 m	0.80	Rod length 3–4 m
			0.85	Rod length 4 – 6 m	0.85	Rod length 4–6 m
			0.95	Rod length 6 – 10 m	0.95	Rod length 6–10 m
			1.00	Rod length 10–30 m	1.00	Rod length 10–30 m
C_S	Standard Sampler	$C_s = 1$	Standard Sampler	$C_s = 1$	Standard Sampler	$C_s = 1$
	Non-Standard Sampler	$C_s = 1 + \frac{N_{1,60}}{100}$ $1.1 \leq C_s \leq 1.3$	Non-Standard Sampler	$C_s = 1 + \frac{N_{1,60}}{100}$ $1.1 \leq C_s \leq 1.3$	Non-Standard Sampler	$C_s = 1.2$
C_E	$C_E = \frac{ER}{60\%}$		$C_E = \frac{ER}{60\%}$		$C_E = \frac{ER}{60\%}$	
C_B	1.00	65mm≤B≤115mm	1.00	65mm≤B≤115mm	1.00	65mm≤B≤115mm
	1.05	B = 150 mm	1.05	B = 150 mm	1.05	B = 150 mm
	1.15	B = 200 mm	1.15	B = 200 mm	1.15	B = 200 mm

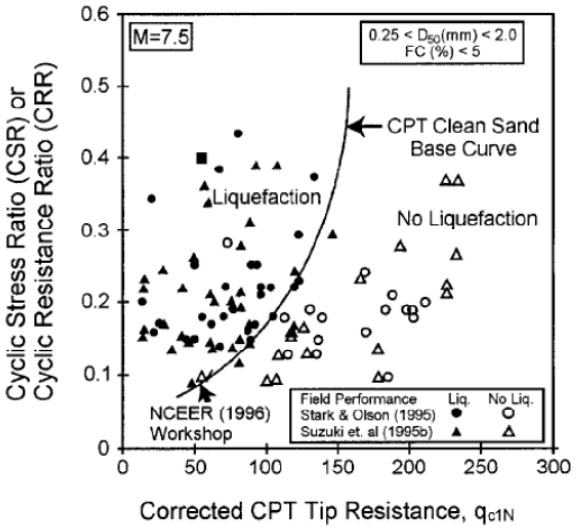

Figure 5: Curve Recommended for Calculation of CRR from CPT Data along with Empirical Liquefaction Data from Compiled Case Histories (Youd et al. 2001, Reproduced from Robertson and Wride 1998)

Seed et al. (2003) state that the CPT-based correlation of Robertson and Wride is slightly unconservative for clean sands, especially at high CSR, and that it is very unconservative for soils of increasing fines content and plasticity. This was verified by comparison with newer CPT-based correlations that are presented and described in the sections that follow and which were based on more recent liquefaction case histories where liquefaction was observed in sites with CPT soundings.

As a result of the above shortcomings, a decision was made not to include the CPT-based liquefaction procedure presented in Youd et al. (2001) in this paper.

2.3.2. Seed et al. (2003) Method

In the CPT-based liquefaction method proposed by Seed et al. (2003), the Cyclic Resistance Ratio (CRR) is determined based on a probabilistic approach as a function of a modified normalized CPT tip resistance $q_{c,1,mod}$, as presented in Figure-6. The normalized CPT tip resistance $q_{c,1,mod}$ is calculated using Equation-21 which includes a correction for fines content reflected in the CPT friction ratio R_f such that:

$$q_{c,1,mod} = q_{c,1} + \Delta q_c \tag{21}$$

where $q_{c,1}=C_q.q_c$ is the normalized tip resistance and Δq_c is a correction factor for the presence of fines. The factor C_q is calculated as $C_q=(P_a/\sigma'_v)^c$, where P_a is the atmospheric pressure and c is an exponent that is calculated from Figure-7a as a function of R_f and $q_{c,1}$. The fines correction factor Δq_c is given in Figure-7b, also as a function of R_f and $q_{c,1}$. It should be noted that the friction ratio to be used in Figure-7 is defined as $R_f=100x(f_{s,1}/q_{c,1})$. The normalized sleeve friction is calculated as $f_{s,1}=C_f\ f_s$, where C_f is a correction factor that is

determined as $C_f=(P_a/\sigma'_v)^s$, where s is an exponent that is determined from Figure-7a.

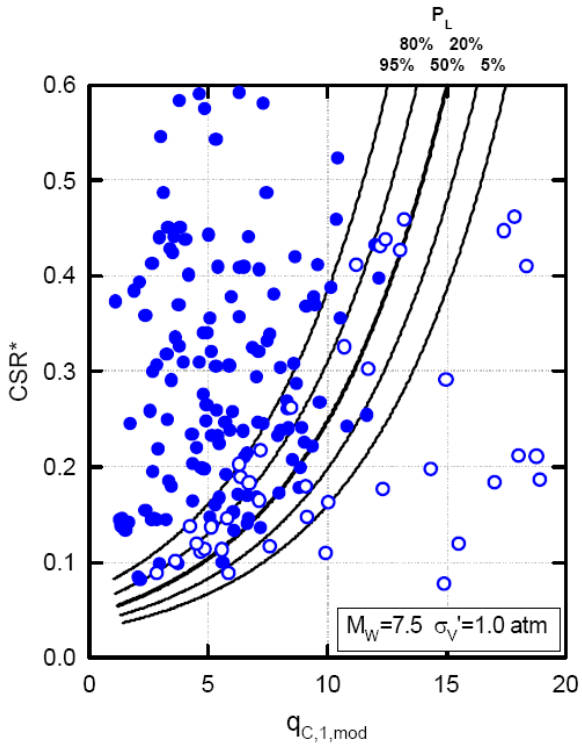

Figure 6: Contours of 5%, 20%, 50%, 80% and 95% Probability of Liquefaction as a Function of Equivalent Uniform Cyclic Stress Ratio and Fines-Modified CPT Tip Resistance (M_w=7.5, σ'_v=1atm.)

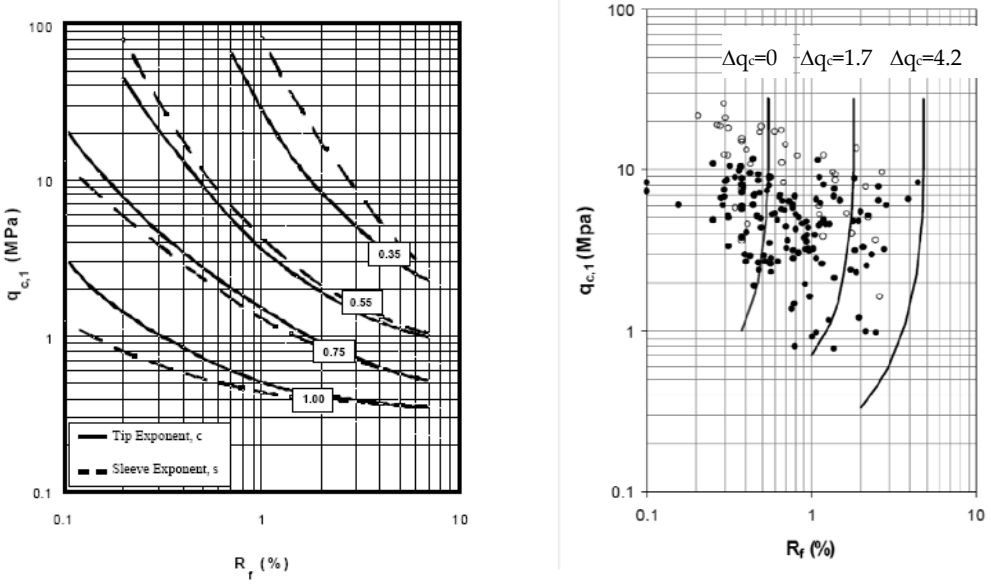

(a) (b)

Figure. 7: (a) Recommended CPT tip and sleeve normalization exponents, and (b) Recommended CPT tip resistance modification for "fines content and character" as a function of $q_{c,1}$ and R_f.

As with their SPT-based approach, Seed et al. (2003) recommend the use of a probability of liquefaction of 15% in the determination of the CRR to evaluate a factor of safety against liquefaction $FS_{liq}=CRR/CSR^*$ that is equivalent to conventional deterministic approaches for liquefaction assessment.

2.3.3. Idriss and Boulanger (2008) Method

In the CPT-based Idriss and Boulanger (2008) liquefaction approach, the cyclic resistance ratio (CRR) is calculated according to the following equation:

$$CRR_{M=7.5,\sigma'_{vc}=1} = \exp\left(\frac{q_{c1Ncs}}{540} + \left(\frac{q_{c1Ncs}}{67}\right)^2 - \left(\frac{q_{c1Ncs}}{80}\right)^3 + \left(\frac{q_{c1Ncs}}{114}\right)^4 - 3\right) \quad (22)$$

where q_{c1Ncs} is given as a function of $q_{c1N} = C_N q_c/P_a$ and the fines content FC:

$$q_{c1Ncs} = q_{c1N} + \left(5.4 + \frac{q_{c1N}}{16}\right).\exp\left(1.63 + \frac{9.7}{FC + 0.01} - \left(\frac{15.7}{FC + 0.01}\right)^2\right) \quad (23)$$

where the normalization constant C_N is calculated as:

$$C_N = \left(\frac{P_a}{\sigma'_{vc}}\right)^{1.338 - 0.249\,(q_{c1N})^{0.264}} \leq 1.7 \quad (24)$$

The factor of safety against liquefaction is then calculated according to:

$$FS_{liq} = \frac{CRR_{M=7.5,\sigma'_{vc}=1}}{CSR_{M=7.5,\sigma'_{vc}=1}} \quad (25)$$

3. Methods for the Assessment of Liquefaction-Induced Settlements

Liquefaction is typically associated with considerable settlements which may cause significant damage to structures and infra-structure. As such, and in order to complete the assessment of the response of a given site to seismic shaking, an estimation of the liquefaction-induced settlements is typically required. Calculation methods for liquefaction-induced settlements in sands generally utilize SPT data as a basis for settlement prediction. Commonly used SPT-based settlement prediction methods are presented in sections 3.1 and 3.2 below for cases involving dry (sands above the water table) and wet sands (sands below the water table), respectively. For cases where the data available is limited to CPT soundings, the correlation presented in Figure-8 could be utilized to estimate the SPT N-value from the CPT tip resistance q_c as a function of the mean grain size D_{50}.

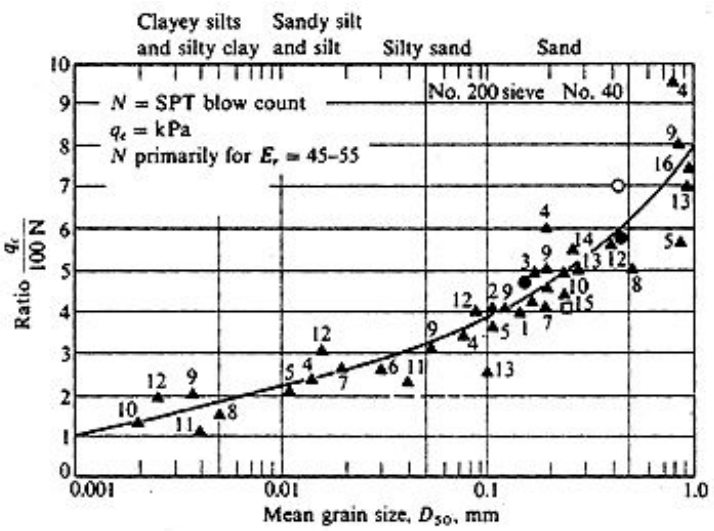

Figure 8: Correlation between the mean grain size and the ratio of the CPT tip resistance to the SPT N-value (after Robertson et al. 1983 and Ismael and Jeragh 1986).

3.1. Settlement Calculations for Dry Sand

The settlement estimates for dry granular materials are obtained from the procedure presented in Tokimatsu and Seed (1987). In this procedure, the Cyclic Shear Stress (τ_{av}) is initially calculated as:

$$\tau_{av} = 0.65\,\frac{a_{max}}{g}\,\sigma_o\,r_d \tag{26}$$

where r_d is the stress reduction coefficient that is calculated from Equation-2. The Shear Modulus (G_{max}) is then calculated as a function of the normalized SPT value N_1 such that:

$$G_{max} = 447\,p_o(N_1)^{1/3}\sqrt{\frac{p}{p_o}} \tag{27}$$

where p_o is the reference atmospheric pressure taken as 95.76 KPa and p is the effective stress calculated as p=0.67$\rho.z$, where ρ is the soil's unit weight and z is the depth at which p is estimated. The Cyclic Shear Strain (γ) is then calculated from Equation-28 calculated as follows:

$$\gamma = \left(\frac{1 + a\,e^{b\,\frac{\tau_{av}}{G_{max}}}}{1+a}\right) \tag{28}$$

where a = 0.0389(p/p_o)+0.124 and b = (6400p/p_o)$^{-0.6}$.

The Volumetric Strain (ε_{Nc}) is then calculated according to Equation-29 as a function of N_c = (M-4)$^{2.17}$ and ε_{15} = γ (N_1/20)$^{-1.2}$ such that:

$$\varepsilon_{Nc} = \varepsilon_{15}\left(\frac{N_c}{15}\right)^{0.45} \tag{29}$$

Eventually, the dry settlement (ΔS) is calculated as a function of the thickness of the layer Δh as:

$$\Delta S = 2\,\Delta h\,\varepsilon_{Nc} \tag{30}$$

3.2. Settlement Calculations for Wet Sand

The calculation of the settlement in "wet sands" is done in accordance with the method proposed by Ishihara and Yoshimi (1992). First, the normalized SPT $(N_1)_{60}$ is converted into relative density D_r using Table-3. Second, the Maximum Cyclic Shear Strain (γ_{max}) is calculated from Figure-9a (Zhang et al., 2004) as a function of the factor of safety against liquefaction. Then the Volumetric Strain (ε_v) is calculated from Figure-9b (Ishihara & Yoshimi 1992) as a function of the maximum shear strain. Finally, the settlement is calculated according to Equation-31:

$$Ssat = \left(\frac{\varepsilon_v}{100}\right) dz \tag{31}$$

where ε_v is the volumetric strain and *dz* is the thickness of the layer.

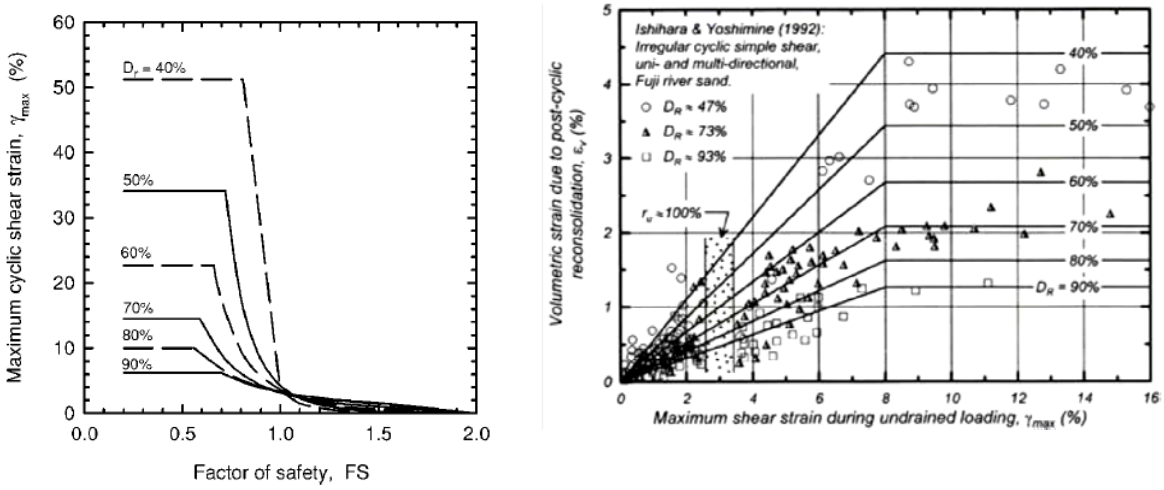

(a) (b)

Figure 9: (a) Relationship between cyclic shear strain and factor of safety and (b) relationship between volumetric strain and cyclic shear strain value.

4. LiqFactory v1.0 Spreadsheet

As was evident from the previous sections, the methods available for liquefaction assessment are quite complex and tedious to implement. We recognized the need to provide students with an accessible platform for using, testing and practice-driven understanding of these methods. The main objective was to provide a state of the practice platform for teaching and real-world applications. The tool would allow a quick solution of any liquefaction related problem using various reputed and acknowledged methods, and for an easy and point by point comparison of the results they yield. A spreadsheet-based approach was selected as the most accessible and effective solution. The information provided and the format it is presented in should allow for a clearer understanding of the "hazard" and a more reliable and comprehensive decision making process in reference to the need for, and extent of, mitigation measures.

It is important to note here that the developed spreadsheet was done in the context of an educational activity. It came as a result of discussions and feedback with students at the completion of a course on geotechnical earthquake engineering, where the methods for evaluating liquefaction potential were introduced. The intricacies and complexities of implementation of these methods on multiple points/depths within a soil profile were highlighted in the student feedback. The use of "black-box" commercial software, which cover some but not all the methods presented, was seen by some students as effective, but did not allow them to appreciate/understand the various input variables, assumptions and procedures involved. The tool described herein has since been used to support that same course with very positive reactions from the students.

4.1. Graphical User Interface (GUI) Forms

The procedures presented in the previous sections for the assessment of liquefaction potential and liquefaction-based settlements were programmed into a spreadsheet that was equipped with a user-friendly graphical user interface. The different components of the interface are presented in the sections below.

4.1.1. Soil Profile

The user is first asked to fill the "Edit Soil Profile" form. It allows the input of the subsurface profile for the case to be analyzed. A capture of this form is presented in Figure-10. The user inputs the number of soil layers within the profile. The number of layers is entered using the "Update" button. If the user wants to edit the number of soil layers at a later stage, he/she can do that using the "Edit" button. Information about the water table is entered next. The depth of the water table is taken from the level of the ground surface.

The next step involves entering the properties of the different layers. For each layer, the user enters all the parameters as shown in Figure-10. The "Layer #" drop box allows the user to select the layer. The box directly next to the drop box is the color used by the sheet to represent the selected layer. The color assigned to any layer can be changed by scrolling and selecting.

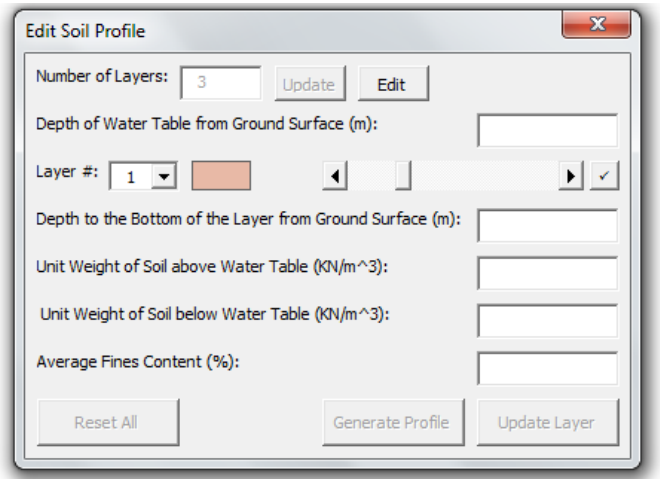

Figure 10: Screen shot of the "Edit Soil Profile" form.

In addition to the color, the user has to enter four parameters for each layer. These are: the depth to the bottom of the layer measured from the ground surface, the unit weights above and below the water table, and the average fines content. Note that the last layer is considered to have infinite depth although the form asks for a value in order to represent it in the "User Interface" Sheet. To update the values to the selected layer, the user should press "Update Layer". Eventually, when the user enters the values for the last layer, the "Generate Profile" button becomes activated. This button draws the user's soil profile on which the analyses will be based. The form tests for odd values like negative numbers, letters and the like. The "Reset All" button deletes all the values in the form and the spreadsheet's memory.

4.1.2. Earthquake Data

The form in which the user inputs the earthquake data is presented in Figure-11. Two parameters are of interest when it comes to studying liquefaction. These are the earthquake magnitude and the peak horizontal ground surface acceleration. The latter should be input as a multiple of the gravitational acceleration "g".

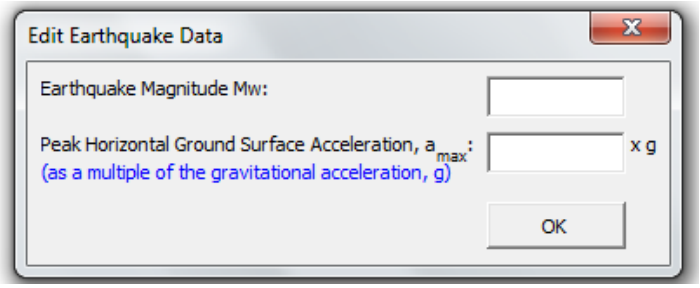

Figure 11: Screen shot of the "Edit Earthquake Data" form.

4.1.3. SPT Data

The "Add SPT Data" form is shown in Figure-12. The SPT data is input in columns. The first column includes the depth while the second includes the

corresponding field (uncorrected N) or corrected (N1,60) SPT number. A third column should include the fines content associated with each depth.

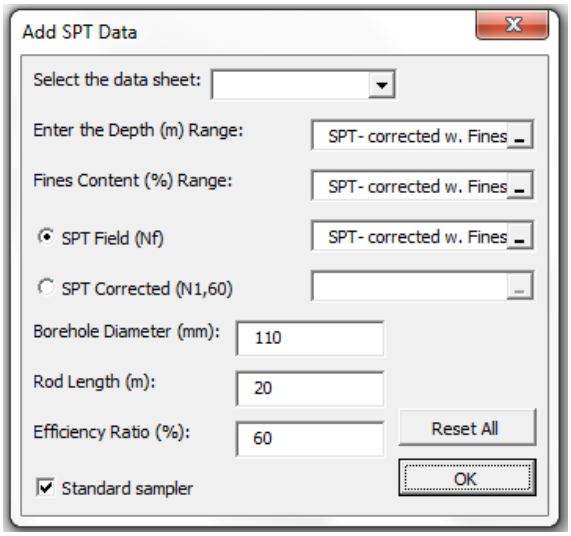

Figure 12: Screen shot of the "Add SPT Data" form.

The "data sheet" drop box allows users to select the sheet in which the data are found. Once the sheet is selected, it will automatically be activated. Once the sheet is activated, the users can select the depth range, the associated SPT N-values, and the associated fines content using the typical Excel range selection method. Note that users have the option of entering either field or corrected SPT number of blows. In case the field SPT values are entered, then they should also enter the borehole diameter, rod length and efficiency ratio in the corresponding text boxes as shown in Figure-12 to allow for the computation of the appropriate correction factors. Moreover, the user needs to determine whether the sampler is standard or not using the check box. The form checks if the number of data in each range is the same once the "OK" button is pressed.

4.1.4. CPT Data

The procedure for adding CPT data is similar to that of the SPT. The user selects the sheet in which the relevant data is found. Then, they need to select the ranges of the depth, cone penetration tip resistance, and sleeve friction (Figure-13).

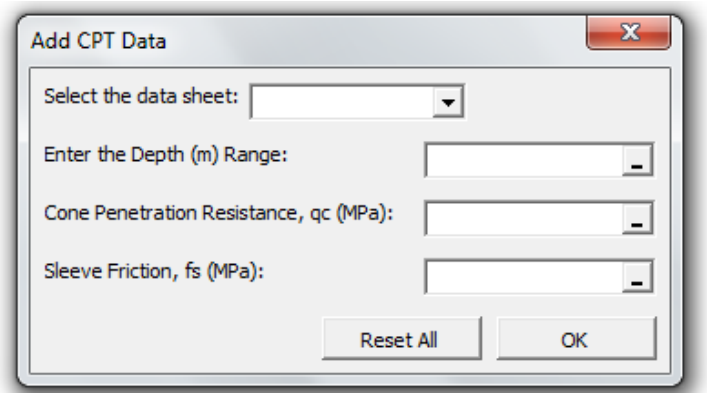

Figure 13: Screen shot of the "Add CPT Data" form.

4.1.5. Draw Graphs

Figure-14 shows the "Draw Graphs" form that allows the user to plot the results of the liquefaction assessment based on both SPT and CPT data. The users have two options in which they would either plot a default layout for the graphs (as arranged in the "Available graphs" list) or change this layout using the arrow buttons between the two lists (i.e. "Available graphs" and "Graphs to be drawn" lists). Note that users can only select the graphs that are of interest to them when choosing the "Choose the graphs and their order" option. After deciding on a certain option, the users can draw the graphs using the "Draw SPT Graphs" button. Similarly, users can plot the graphs related to CPT data by selecting the "CPT" tab. The users can also delete the existing graphs by selecting the option button "Choose the graphs and their order:" and pressing directly on "Draw SPT/CPT Graphs" button while leaving the "Graphs to be drawn" list empty.

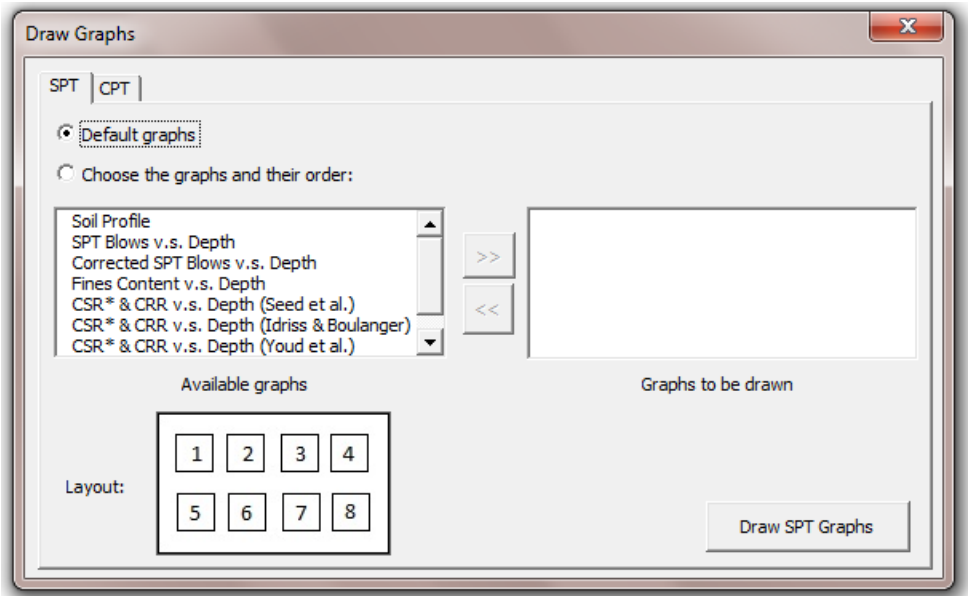

Figure 14: Screen shot of the "Draw Graphs" form.

4.1.6. Compute Settlements

Figure-15 shows the "Compute Settlements" form. The users select to compute settlements based on either SPT or CPT data. If CPT data is used, the user should enter the mean grain size D_{50} to be used in the correlation presented in Figure-8 to convert the CPT tip resistance into an equivalent SPT N-value.

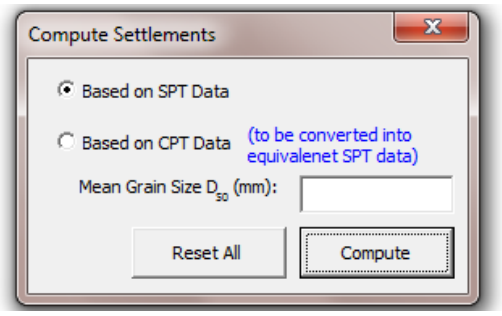

Figure 15: Screen shot of the "Compute Settlements" form

4.2. Programming Challenges and Assumptions

To limit the length of this paper, the discussion related to the programming effort that was associated with designing the spreadsheet from a computational perspective will be restricted to the challenges and assumptions that were faced/made. Where relevant, the code that was developed to solve the challenges is presented.

4.2.1. SPT-Based Methods

A common challenge that was faced in almost all the methods was the need for finding mathematical expressions that would represent some of the graphical solutions that required programming. In general, the solution to this challenge was through digitization of empirical relationships and using numerical fitting schemes. Examples of relationships which required digitization in the SPT-based methods are the relationships required to estimate r_d, *DWF*, K_{sigma}, and *CRR*. In what follows is a brief presentation of some useful expressions that resulted from that effort.

r_d-mean (Seed et al. 2003)

The curve of $r_{d(mean)}$ was digitized from Figure-2 and a 5th order polynomial was used to determine a relationship between the depth *z* and the reduction factor r_d (Equation-32). The expression which provides *z* as a function of r_d was found to provide a better fit to the graphical relationship as opposed to the more conventional approach in which r_d is established as a function of *z*. The challenge in solving for r_d using Equation-32 was solved by writing a code that iterates for r_d in the range of 0.2 and 1.1 until the calculated depth from Equation-32 is equal to the desired depth *z* at which r_d is required. Note that a traditional relationship that would result in a value of r_d as a function of depth could have been used; however, the accuracy of the results in this case was found to be smaller than the procedure implemented in the spreadsheet.

$$z = -9941.6(r_d)^5 + 40637(r_d)^4 - 66574(r_d)^3 + 54499(r_d)^2 - 22312(r_d) + 3690.5 \quad (32)$$

DWF and K_{sigma} (Seed et al. 2003)

A similar procedure was followed in digitizing the curves which relate the duration weighting factor DWF_M with the earthquake magnitude in Figure-3a and the overburden correction factor K_{sigma} to the vertical effective stress σ'_v (in psf) in Figure-3b. Power functions were used to fit the curves once digitized. This resulted in the relationships presented in Equations 33 and 34:

$$DWF_M = 92.487(M_w)^{-2.251} \quad (33)$$

$$K_{sigma} = 7.69\left((20885.46\sigma'_v)^{-0.268}\right) \quad (34)$$

CRR Curve (Seed et al. 2003)

The solution of Seed et al. (2003) for determining a relationship between the CRR and $N_{1,60,CS}$ is probabilistic in nature and was presented for probabilities of liquefaction of 5%, 20%, 50%, 80%, and 95%. However, Seed et al. (2003) recommend a probability of liquefaction of 15% to be equivalent to the deterministic approaches. To estimate the curve that corresponds to the 15th percentile liquefaction potential, a manual curve was interpolated and drawn between the 5th and 20th percentile curves and the image with the new interpolated curve was scanned and saved. The scanned image was then used to digitize the 15th percentile liquefaction curve and a 6th order polynomial (Equation-35) was used to provide a best fit for the relationship between CRR and the corrected SPT blow count $N_{1,60,CS}$:

$$CRR = 2e^{-10}(N_{1,60,CS})^6 - 2e^{-8}(N_{1,60,CS})^5 + 1e^{-6}(N_{1,60,CS})^4 - 2e^{-5}(N_{1,60,CS})^3 + 4e^{-4}(N_{1,60,CS})^2 - 9e^{-4}(N_{1,60,CS}) \quad (35)$$

CRR curve (Youd et al. 2001)

The solution of the SPT-based Youd et al. (2001) method as reflected in Figure-1 includes curves for clean sands, sands with a fines content of 15% and sands with a fines content of 35%. To program the graphical solution into the spreadsheet, mathematical relationships were derived for cases with intermediate fines content (at intervals of 2.5% for FC between 5% and 15% and at intervals of 5% for FC between 15% and 35%) as illustrated in Equations 36 to 45. The curves for intermediate fines content were drawn by hand, digitized, and fitted with 2nd degree polynomials. Since, the upper bound of these relationships includes the case with $N_{1,60}$ of 30, it was assumed in the spreadsheet that the cyclic resistance ratio (CRR) is equal to 0.6 whenever $N_{1,60}$ was greater than 30. On the other hand, when $N_{1,60}$ is less than 30, Equations 36 to 45 are used to relate between CRR and $N_{1,60}$ for different fines contents. The code takes FC = 5% as a lower bound and FC = 35% as an upper bound. It is worth noting that Equations 36 to 45 present $N_{1,60}$ as a function of the CRR. This decision was made to produce better fits for the

curves in Figure-1 and the solution of these equations could be obtained using the procedure presented to solve for $r_{d,mean}$ in the section above.

For FC <= 5%, $N_{1,60} = -154.45(CRR)^2 + 143.18(CRR) - 3.9327$ (36)

For FC > 5% and FC <= 7.5% $N_{1,60} = -139.54(CRR)^2 + 133.53(CRR) - 3.9347$ (37)

For FC > 7.5% and FC <= 10% $N_{1,60} = -135.96(CRR)^2 + 129.93(CRR) - 4.4052$ (38)

For FC > 10% and FC <= 12.5% $N_{1,60} = -132.19(CRR)^2 + 126.65(CRR) - 4.9595$ (39)

For FC > 12.5% and FC <= 15% $N_{1,60} = -125.99(CRR)^2 + 121.83(CRR) - 5.3565$ (40)

For FC > 15% and FC <= 20% $N_{1,60} = -127.40(CRR)^2 + 121.53(CRR) - 5.6843$ (41)

For FC > 20% and FC <= 25% $N_{1,60} = -125.73(CRR)^2 + 119.27(CRR) - 6.0563$ (42)

For FC > 25% and FC <= 30% $N_{1,60} = -126.94(CRR)^2 + 118.41(CRR) - 6.3398$ (43)

For FC > 30% and FC <= 35% $N_{1,60} = -119.80(CRR)^2 + 114.5(CRR) - 6.6814$ (44)

For FC > 35% $N_{1,60} = -119.80(CRR)^2 + 114.5(CRR) - 6.6814$ (45)

4.2.2. CPT-Based Methods

A major challenge was faced in programming the CPT-based procedure presented in Seed et al. (2003) in relation to calculating the tip exponent *c* and the sleeve exponent *s*, which are needed to correct the tip resistance q_c and the sleeve friction f_s. The exponents could be obtained graphically from Figure-7a as a function of the friction ratio R_f and the normalized tip resistance $q_{c,1}$. Since the calculation of $q_{c,1}$ and R_f requires knowledge of *c* and *r*, an iterative solution was required to determine these exponents.

As a first step in the solution, the curves of the tip exponent *c* and the sleeve exponent *s* were separated into two figures as indicated in Figure 16a and 16b below. For each graph, 9 curves representing different values of c and s were interpolated between the 4 curves published in Seed et al. (2003) to bring the total number of curves in each graph to 13. A total of 26 curves were then digitized in preparation for fitting mathematical expressions to them. In the process, and because of the logarithmic scale, it was noticed that the best fit to the curves is obtained if each of the curves is split into two parts: the first representing friction ratios R_f between 0.1% and 1% and the second representing R_f values between 1% and 10%. Hence, a total of 52 mathematical expressions were used to model the curves in Figure-16.

The solution to the iteration problem starts from a first guess for the exponent *c*, calculating R_f (from the 52 equations), and comparing it to the actual R_f. The programmed function loops for the other values and calculates a new R_f each time until the difference between the calculated R_f and the actual R_f becomes small. The lower bound for *c* and *s* is 0.35 whereas the upper bound is 1.

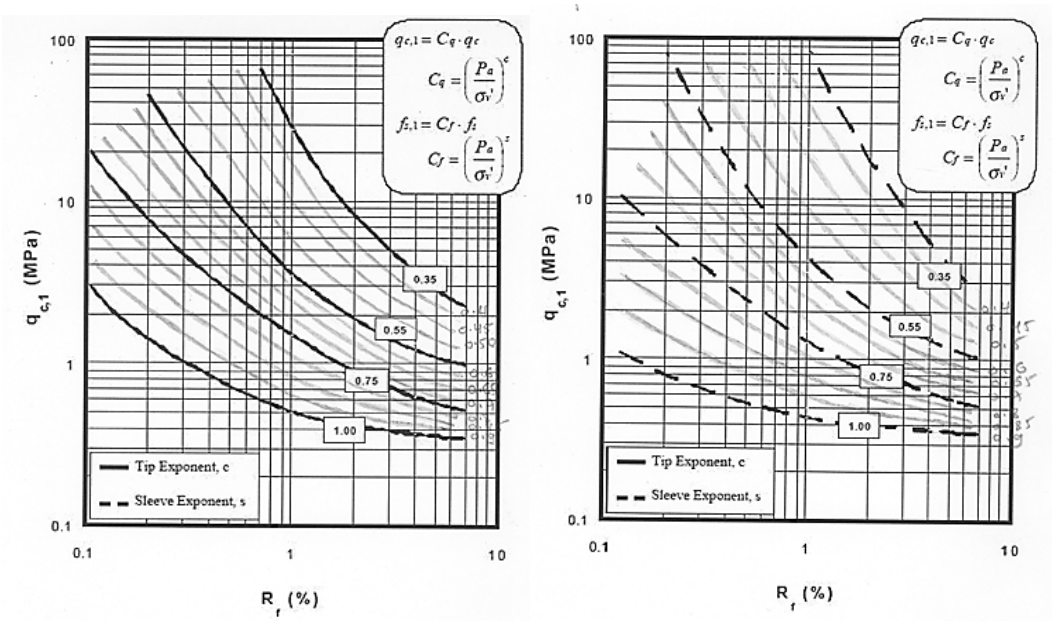

(a) (b)

Figure 16: Interpolated curves for (a) Tip Exponent *c*, and (b) Sleeve Exponent *s*

4.2.3. Settlement Calculations

Conversion from CPT to SPT (wet settlement)

Equation-46 shows the mathematical expression that was used to fit the correlation between CPT and SPT as presented in Figure-8. It should be noted that the lower bound for the ratio $q_c/100N$ was taken as 1 while the upper bound was taken as 8.

$$\frac{q_c}{100N} = 7.6508\left(D_{50}\right)^{0.2801} \tag{46}$$

Maximum Cyclic Shear Strain (γ_{max}, wet settlement)

The relationship between the maximum shear strain γ_{max} and the factor of safety FS is presented in Figure-9a with different relationships shown for different relative densities. To model the graphical solution using mathematical equations, the relationship for each relative density was divided into three different parts: the first part represents the low values of the factor of safety where γ_{max} is assumed to be a constant. For this part, the value of γ_{max} is interpolated between the given curves according to the relative density (D_r). The second part is for intermediate factors of safety with an upper bound of 1. In this part, the relationship between FS and γ_{max} is assumed to be linear and accordingly the curves were digitized and fitted with linear functions that were used as a basis of the interpolation according to the value of D_r. The last and third part is for FS greater than 1. The relationship between FS and γ_{max} was considered to be linear and independent of D_r. As a result, only one curve was digitized and fitted with a linear function to represent the relationship

between FS and γ_{max}. The upper bound for the relative density was taken as D_r = 90% whereas the lower bound was taken as D_r = 40%.

Volumetric Strain (ε_v , wet settlement)

A similar approach was used to represent the graphical solution of the volumetric strain (Figure-9b) using mathematical expressions. In the process, the curves were divided into two linear segments. The first linear part represents maximum cyclic shear strain γ_{max} less than 8% where linear interpolation was used to obtain results for different relative densities. The second segment is for γ_{max} greater than 8%, where for a specific value of D_r, ε_v is constant regardless of the value of γ_{max}. In the formulation, the upper bound is taken as D_r = 90% whereas the lower bound is taken as D_r = 40%.

5. Illustrative Example

This section is dedicated to demonstrate the use of the Software through an illustrative example. The example is based on a real-world project where a liquefaction assessment was required, and which is used as a hands-on application exercise in the geotechnical earthquake engineering course.

5.1. Soil Profile and Properties

The case study under investigation involves a site located along the Lebanon coast. The top 5 to 6 meters of the site are reclaimed from the sea and consist of fill that could be characterized as a medium dense to dense silty sand with gravels and cobbles. The fill is underlain by natural soils that consist of very loose to dense silty and clayey sands up to depths of about 17 to 18m. A relatively hard marl/limestone layer exists under the silty/clayey sands. A representative soil profile is shown in Figure-17. Note that the water table is taken to be at ground level. Standard penetration test and cone penetration test data were available for the site. The available data is presented in Figure-18 and Figure-19 for SPT and CPT tests, respectively. Information about fines content and unit weight is presented in Figure-17.

Figure 17: Soil profile of the illustrative example

The first step consists of inputting the general soil properties and the earthquake data into the spreadsheet. This step is completed following the instructions indicated in Sections 4.1.1 and 4.1.2. The second step is to enter the SPT and CPT data as indicated in Sections 4.1.3 and 4.1.4. The software automatically performs the necessary computations and a summary of the results of the liquefaction assessment is obtained for the SPT and the CPT-based methods, respectively. The user is then prompted to select corresponding graphs for the SPT and CPT-based results and to obtain the vertical settlement based on either the SPT or CPT data.

5.2. SPT-based Methods

The output of the liquefaction assessment is presented in Figure-18 for the three SPT-based liquefaction methods. The output consists of two sets of graphs: the first set summarizes the input properties including the soil profile in addition to graphs showing the variation of field SPTs, corrected SPTs, and fines content with depth. The second set includes the variation of the CSR and the CRR with depth for the different methods in addition to the variation of the resulting factor of safety with depth. For the example considered, the earthquake magnitude M_w was taken to be equal to 7.5 and the Peak Ground Acceleration was taken as 0.25g as indicated in the applicable local codes of practice.

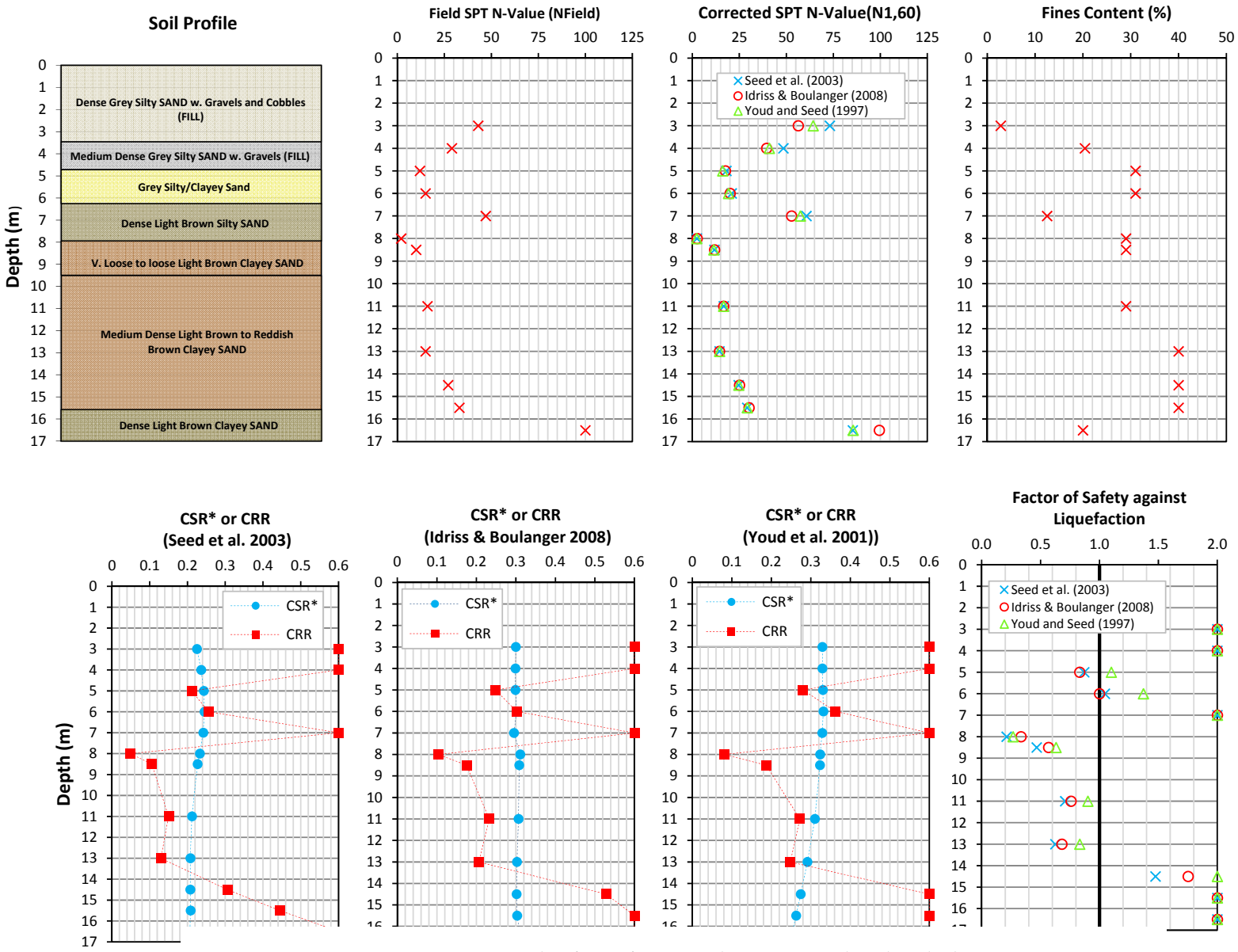

Figure 18: Results of Liquefaction Analysis using SPT-based Methods

Results shown in Figure-18 indicate factors of safety against liquefaction that are less than 1.0 at a depth of 5.0m and at depths between 8.0 and 13.0m. These depths were characterized by relatively low SPT values (generally less than 15). For this particular site, the risk of liquefaction as reflected in the factor of safety was similar for the three SPT-based methods, despite slight variations in the magnitudes of the computed factors of safety at different depths. It should be noted that whenever the computed factor of safety was greater than 2, it was plotted as 2 in the output graphs so as not to disrupt the scale of the x-axis in the figure.

In general, results indicate that the method of Seed et al. (2003) results in factors of safety that are generally smaller than those calculated by the other two methods. The difference however is generally in the range of 10% to 20%. The largest difference in the calculated factors of safety between the three methods was observed for a depth of 14.5m, where the factor of safety was calculated as 1.47 for the Seed et al. (2003) method, 1.75 for the Idriss and Boulanger (2008) method, and about 2.0 for the Youd et al. (2001) method.

Despite some differences in the calculated factors of safety, all SPT-based methods predicted the depths at which liquefaction is probable.

5.3. CPT-based Methods

The CPT sounding presented in Figure-19 was used to predict the liquefaction potential at the site using the CPT-based methods of Seed et al. (2003) and Idriss and Boulanger (2008). The variations of the cone penetration resistance q_c and the friction ratio f_s with depth are also presented in Figure-19, which constitutes the output graph for the CPT-based analysis. As with the SPT-based methods, the output also includes the variation of the CSR and the CRR with depth for the different methods in addition to the variation of the resulting factor of safety with depth.

The results of the CPT-based liquefaction analysis indicate the potential occurrence of liquefaction between depths of 5m and 6m and at depths below 9.0m, where relatively low cone trip resistance values q_c were measured. Both methods predicted liquefaction at the above-mentioned depths, with the calculated factors of safety at all depths being relatively similar indicating consistency in the results of the two CPT-based methods for this particular example.

A thorough examination of the results on Figure-19 indicate that the Seed et al. (2003) method resulted in slightly lower factors of safety at relatively shallow depths in comparison to the Idriss and Boulanger (2008) method, while the latter resulted in slightly lower factors of safety at relatively larger depths.

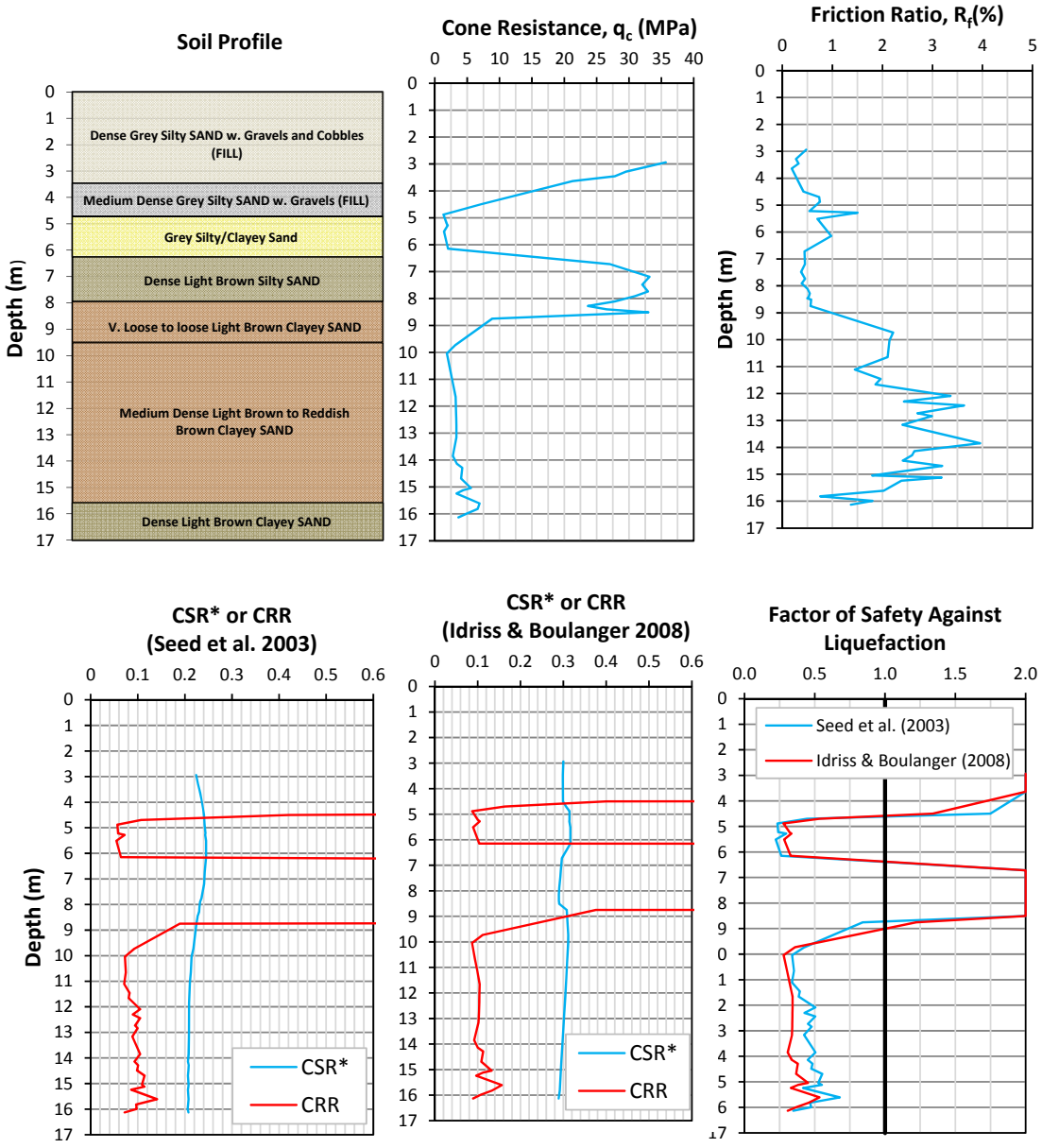

Figure 19: Results of Liquefaction Analysis using CPT-based Methods

5.4. Settlement Computation

The excel-based tool documented in this paper can calculate the vertical settlement based on SPT data. This can be done through using the SPT data (Youd et al. 2001) directly or by converting the CPT data to SPT data. The software detects the position of the water table and calculates the dry settlement above it and the wet settlement below it. In this example the water table is at the ground level so only the wet settlement is calculated for the different layers. Table 5 shows the output of the vertical settlement that is calculated using the SPT data directly. The total settlement is around 16.4 cm.

Table 5: Settlement computation based on SPT

			Settlement in Wet Soil				Total Settlement
Depth (m)	$N_{1,60}$	FS	D_r	γ_{max} (%)	ε_v	Δs (m)	$\Sigma \Delta s$ (m)
3	64.22	3.06	90	0	0	0.000	0.000
4	40.92	2.75	90	0	0	0.000	0.000
5	16.11	1.10	63.4	2.3	0.71	0.007	0.007
6	19.24	1.37	69.1	1.2	0.32	0.003	0.010
7	57.43	2.24	90	0	0	0.000	0.010
8	2.33	0.27	30	51.3	4.42	0.044	0.055
8.5	11.42	0.63	53.8	31.2	3.15	0.016	0.070
11	16.61	0.90	64.3	5.4	1.64	0.041	0.111
13	14.46	0.83	60.2	8	2.66	0.053	0.164
14.5	24.71	2.03	79	0	0	0.000	0.164
15.5	29.22	2.07	88.1	0	0	0.000	0.164
16.5	85.48	2.11	90	0	0	0.000	0.164

6. Conclusions

In this paper, a spreadsheet that is equipped with a user-friendly graphical user interface was developed to provide an efficient tool for analyzing liquefaction problems using state-of-the-knowledge methods that are available in the literature for assessing the liquefaction potential of granular soils. The technical background associated with the spreadsheet was presented and the challenges associated with the development of the spreadsheet were discussed. A step-by-step procedure for using the spreadsheet is presented to facilitate the use of the software by engineers or engineering students. Finally, a real-world practical example was introduced to illustrate the added value brought by the spreadsheet and to provide users with an idea of the results that could be obtained from the spreadsheet.

7. References

Andrus, R.D., and Stokoe, K.H., II. (1997). "Liquefaction Resistance Based on Shear Wave Velocity", *Proceedings, NCEER Workshop on Evaluation of Liquefaction Resistance of Soils*, National Center for Earthquake Engineering Research., State University of New York at Buffalo, 89–128.

Cetin, K.O., Seed, R.B., Kiureghian, A.D., Tokimatsu, K., Harder, L.F., Kayen, R.E., and Moss, R.E.S. (2004). "Standard Penetration Test-Based Probabilistic and Deterministic Assessment of Seismic Soil Liquefaction Potential", *Journal of Geotechnical and Geoenvironmental Engineering*, ASCE, Vol.130, 1314-1340.

Idriss, I. M. (1995). H. B. Seed Memorial Lecture, Univ. of CA, Berkeley.

Idriss, I. M. and Boulanger, R. W. (2008). "Soil Liquefaction during Earthquakes", Earthquake Engineering Research Institute (EERI), Oakland, California.

Ishihara, K., and Yoshimi M. (1992). "Evaluation of Settlements in Sand Deposits following Liquefaction during Earthquakes", *Soils and Foundations*, Vol. 32, No. 1, 173‐188.

Ismael, N. F., and Jeragh, A. M. (1986). "Static Cone Tests and Settlement of Calcareous Desert Sands", *Canadian Geotechnical Journal*, Vol. 23, 297–303.

Kramer, S. L. (1995). "*Geotechnical Earthquake Engineering*", Prentice Hall PTR, pp. 653.

Pradel, D. (1998). "Procedure to Evaluate Earthquake-Induced Settlements inn Dry Sandy Soils", *Journal of Geotechnical and Geoenvironmental Engineering*, ASCE, Vol. 124, No. 4, 364-368.

Robertson, P. K., Campanella, R. G., and Wightman, A. (1983). "SPT-CPT correlations", *Journal of Geotechnical Engineering*, ASCE, Vol. 109, No.11, 1449–1459.

Robertson, P. K., and Wride, C. E. (1998). "Evaluating Cyclic Liquefaction Potential Using the Cone Penetration Test", *Canadian Geotechnical Journal*, Vol. 35, 442-459.

Seed, H. B. and Idriss, I. M. (1971). "Simplified Procedure for Evaluating Liquefaction Potential", *Journal of the Soil Mechanics and Foundations Division*, ASCE, Vol.107, No.SM9, 1249-1274

Seed, H. B. and Idriss, I. M. (1982). "Ground Motions and Soil Liquefaction During Earthquakes", Earthquake Engineering Research Institute (EERI), Oakland, California.

Seed, R.B., Cetin, K.O., Moss, R.E.S., Kammerer, A.M., Wu, J., Pestana, J.M., Riemer, M.F., Sancio, R.B., Bray, J.D., Kayen, R.E., and Faris, A. (2003). "Recent Advances in Soil Liquefaction Engineering: A Unified and Consistent Framework", Earthquake Engineering Research Center (EERC), Long Beach, California.

Tokimatsu, K., and Seed H. B. (1987). "Evaluation of Settlements in Sand due to Earthquake Shaking", *Journal of Geotechnical Engineering*, ASCE, Vol. 113, No. 8.pp. 861-878.

Youd, T.L., Idriaa, I.M., Andrus, R.D., Argano, I., Castro, G., Christian, J.T., Dobry, R., Liam Finn, W.D., Harder, L.F. Jr., Hynes, M.E., Ishihara, K., Koester, J.P., Liao, S.S.C.,

Marcuson, W.F. III., Martin G.R., Mitchell, J.K., Moriwaki, Y., Power, M.S., Robertson, P.K., Seed R.B., and Stokoe, K.H. II. (2001). "Liquefaction Resistance of Soils: Summary Report from the 1996 NCEER and 1998 NCEER/NSF Workshops on Evaluation of Liquefaction Resistance of Soils", *Journal of Geotechnical and Geoenvironmental Engineering*, ASCE, Vol. 127, No. 10, 819-833.

Zhang, G., Robertson, P.K., and Brachman, R.W.I. (2004). "Estimating Liquefaction-Induced Lateral Displacements using the Standard Penetration Test or Cone Penetration Test", *Journal of Geotechnical and Geoenvironmental Engineering*, ASCE, Vol. 130, No. 8, 861-871.